AD-A273 437

# UMENTATION PAGE

Form Approved
OMB No 0704-0188



| 2. REPORT DATE | 3. REPORT TYPE AND DATES COVERED |
|---|---|
| | ANNUAL 15 Sep 92 TO 14 Oct 93 |

**4. TITLE AND SUBTITLE**

NONLINEAR DYNAMICS APPLIED TO ATMOSPHERIC PREDICTION

**5. FUNDING NUMBERS**

F49620-92-J-0498
61102F
2304/BS

**6. AUTHOR(S)**

Dr Richard L. Pfeffer

**7. PERFORMING ORGANIZATION NAME(S) AND ADDRESS(ES)**

Geophysical Fluid Dynamics
Florida State University
018 Keen Bldg
Tallahassee, FL 32306

**8. PERFORMING ORGANIZATION REPORT NUMBER**

AFOSR-TR- 93 0857

**9. SPONSORING/MONITORING AGENCY NAME(S) AND ADDRESS(ES)**

AFOSR/NL
110 Duncan Avenue, Suite B115
Bolling AFB DC 20332-0001

M&J JAMES T. KROLL

**10. SPONSORING/MONITORING AGENCY REPORT NUMBER**



**11. SUPPLEMENTARY NOTES**

**12a. DISTRIBUTION/AVAILABILITY STATEMENT**

Approved for public release;
distribution unlimited

**12b. DISTRIBUTION CODE**

**13. ABSTRACT** *(Maximum 200 words)*

Under AFOSR grant F49620-92-J-0498, Drs Barcilon and Nathan are studying the impact of steady, zonally varying vorticity forcing on topographic instability and finite amplitude, low frequency oscillations. The model consists of a viscous, barotropic fluid on a zonally periodic, midlatitude B-plane channel, bounded above by a flat, rigid boundary, below by a bottom topography, and laterally by sidewalls at y = o,TT Topographically induced low frequency oscillations in the presence of a steady, zonally varying vorticity source have been studied. The source has been shown to interact with the pertubation field to pruduce zonally rectified wave fluxes that change the zonal momentum balance of the system. This change provides a mechanism for coupling the topographic and vorticity forcings, leading to a dramatic alteration in the Hopf bifurcation from stationary to low frequency, finite amplitude oscillation.

**14. SUBJECT TERMS**

**15. NUMBER OF PAGES**

**16. PRICE CODE**

| 17. SECURITY CLASSIFICATION OF REPORT | 18. SECURITY CLASSIFICATION OF THIS PAGE | 19. SECURITY CLASSIFICATION OF ABSTRACT | 20. LIMITATION OF ABSTRACT |
|---|---|---|---|
| (U) | (U) | (U) | (UL) |

# ANNUAL
# TECHNICAL REPORT

Under

AFOSR Grant 49620-92-J-0498

## Nonlinear Dynamics Underlying Atmospheric Prediction

by

Richard L. Pfeffer
Principal Investigator
Geophysical Fluid Dynamics Institute
Florida State University
Tallahassee FL 32306-3017

August 1993

# I. INTRODUCTION

During the first year of this grant, 4 papers have been completed or are nearing completion based on full or partial support of AFOSR 49620-92-J-0498, including the work of two graduate students, as follows.

Krishnamurti, R., 1993: Generation of Low Frequency Modes in Turbulent Rayleigh-Bernard Convection. To be submitted to *J. Fluid Mech.*

Li, L. and T. R. Nathan, 1993: The global atmospheric response to localized time varying forcing: Zonally averaged basic states. To be submitted to *J. Atmos. Sci.*

Nathan, T. R. and A. Barcilon, 1993: Low frequency oscillations of forced barotropic flow. To be published in *J. Atmos. Sci.*

Zhu, K., I. M. Navon and X. Zou, 1993: Variational Data Assimilation Experiments with Variable Resolution Finite-Element Shallow-Water Equations Model. Submitted to *Mon. Wea. Rev.*

Section II contains abstracts of these papers. Section III contains additional information concerning some of the areas of accomplishment.

# II. ABSTRACTS OF PAPERS

# Generation of Low Frequency Modes in Turbulent Rayleigh-Bernard Convection

by

**Ruby Krishnamurti**
Geophysical Fluid Dynamics Institute
and Department of Oceanography
Florida State University
Tallahassee FL 32306-3017

## Abstract

Laboratory experiments on turbulent Rayleigh-Bernard convection have shown large scale organization of two kinds, the first a steady large scale flow, the second locally periodic travelling clusters of plumes. For Prandtl number $P_r = 7$, the first of these sets in at Rayleigh number $R = 2 \times 10^6$ with the flow in one direction along the bottom and in the opposite direction along the top of the layer (Krishnamurti and Howard 1981). Unlike the cellular flow at low $R$ which has horizontal scale comparable to the layer depth this flow fills the entire width of the tank (which may be 50 times the depth), or may circulate around an annular tank. All the plumes become organized with the same tilt, the hot plumes from the bottom boundary layer drifting in one direction with the large scale flow, the cold plumes from the top drifting in the opposite direction. A measurement of the turbulent velocities and their correlations showed that (Krishnamurti and Howard 1983) the Reynolds stress divergence balances the viscous force on the large scale (horizontally averaged) flow $\overline{u}$:

$$\frac{\partial}{\partial z}\overline{uw} = \nu\frac{\partial^2\overline{u}}{\partial z^2}$$

The tilt of the plumes is such that the momentum transport by the Reynolds stress $\overline{uw}$ is counter to the transport by the viscous stress on the mean flow. In a low order mathematical model (Howard and Krishnamurti 1986) it was shown that tilted flows can result from a symmetry breaking bifurcation from upright cellular flow to one that tilts to the right or to the left.

Even more remarkable is the second kind of organized flow in which this large scale flow becomes locally time periodic for $R \geq 10^7$. There is a spontaneous generation of low frequency modes. These low frequency modes are found both in Hovmuller diagrams and in power spectra of temperature time series. The Hovmuller diagrams shows that clusters of tilted plumes travel as a coherent packet across the convecting layer. These packets of plumes are followed by quiescent regions which are followed by yet another packet and so on. A mathematical model will be presented in which passage of a plume has depleted the thermal boundary layer in a history-dependent way: the boundary layer is very thin where the plume has just passed, but has had time to thicken where the plume passed some time ago. Thus at any moment there is a thermal boundary layer of varying thickness, and the pressure gradient in it drives a flow towards the thicker regions. Taking this to be slow viscous flow, there is then a shear and a down-gradient momentum flux at the wall. This boundary layer is supposed to erupt when and where its thickness reaches some critical

value. Then assuming that the interior momentum flux is entirely by Reynolds stresses, we show by matching interior and boundary layer heat and momentum fluxes, that plumes move away from regions of thick boundary layer at just such a rate that the ever-thickening boundary layer keeps the plume "fed" with buoyant fluid. The predicted period will be shown to be in reasonable agreement with that obtained in the laboratory experiments.

# Low Frequency Oscillations of Forced Barotropic Flow

by

**Terrence R. Nathan**
Atmospheric Science Program
University of California
Davis, CA 95616

and

**Albert Barcilon**
Department of Meteorology and Geophysical Fluid Dynamics Institute
Florida State University
Tallahassee, FL 32306-3017

Submitted to
Journal of the Atmospheric Sciences
*Notes and Correspondence*
August 21, 1992
Revised
July 8, 1993

## Abstract

Jin and Ghil (1990) demonstrate that for topographically resonant flow, low frequency finite-amplitude oscillations may arise from wave-wave interactions and topographic form-drag. Their model is extended to include a zonally asymmetric vorticity source, which is shown to interact with the perturbation field to produce zonally rectified wave fluxes that dramatically alter the Hopf bifurcations from stationary solutions to low frequency oscillations. The frequency, intensity, and general character of these oscillations are shown to depend crucially upon the phasing and relative strength of the forcings.

# Variational Data Assimilation Experiments with Variable Resolution Finite-Element Shallow-Water Equations Model

by

**Keyun Zhu**
Supercomputer Computations Research Institute
Florida State University, Tallahassee, FL 32306-4052

**I. M. Navon**
Department of Mathematics, Geophysical Fluid Dynamics Insitute and
Supercomputer Computations Research Institute
Florida State University, Tallahassee, FL 32306-1307

and

**X. Zou**
Supercomputer Computations Research Institute
Florida State University, Tallahassee, FL 32306-4052

*May 28, 1993*

Submitted to Monthly Weather Review

## Abstract

The adjoint model of a finite-element shallow-water equations model was obtained with a view to calculate the gradient of a cost functional in the framework of using this model to carry out variational data assimilation (VDA) experiments using optimal control of partial differential equations.

The finite-element model employs a triangular finite-element Galerkin scheme (Navon, 1979). The derivation of the adjoint of this finite-element model involves overcoming specific computational problems related to obtaining the adjoint of iterative procedures for solving systems of non-symmetric linear equations arising from the finite-element discretization and dealing with irregularly ordered discrete variables at each time-step.

The correctness of the adjoint model was verified at the subroutine level, and was followed by a gradient check conducted once the full adjoint model was assembled. VDA experiments were performed using model-generated observations. In our experiments, assimilation was carried out assuming that observations consisting of a full-model-state vector are available at every time step in the window of assimilation. Successful retrieval was obtained using the initial conditions as control variables, involving the minimization of a cost function consisting of the weighted sum of difference between model solution and model generated observations.

An additional set of experiments was carried out aiming at evaluating the impact of carrying out VDA involving variable mesh resolution in the finite-element model over the entire assimilation period. Several conclusions are drawn related to the efficiency of VDA with finite element discretization with variable horizontal mesh resolutions and the transfer of information between coarse and fine meshes.

# The Global Atmospheric Response to Localized Low Frequency Forcing: Zonally Averaged Basic States

by

**Long Li and Terrence R. Nathan**

Atmospheric Science Program
Department of Land, Air and Water Resources
University of California, Davis, CA 95616

submitted to
*Journal of Atmospheric Sciences*
August 1993

## Abstract

The remote response to localized, low frequency forcing is examined using a linearized, non-divergent barotropic model on a sphere. Zonal mean basic states characterized by solid body rotation, critical latitudes, reflective surfaces, or wave guides are considered. For slowly varying basic states in which the forcing is located entirely within the tropical easterlies, a WKB and ray tracing analysis shows that in sharp contrast to stationary waves, low frequency waves can propagate through the tropical easterlies into middle latitudes. This propagation is most pronounced for wave periods of 10–20 days. Based on the principle of conservation of wave action, it is shown that as the meridional scale of the wave decreases (increases) the wave amplitude must increase (decrease). An eigenanalysis shows that although both eastward and westward-propagating normal modes are generated by the localized, low frequency forcing, the forcing projects more strongly onto the westward-propagating modes, which are favored for meridional propagation. These results strongly suggest that westward-propagating, low frequency disturbances generated within the tropics may have a more important impact on long-term weather prediction in middle latitudes than previously thought.

# III. SUMMARY OF ACCOMPLISHMENTS

## 1. Low Frequency Dynamics and Predictability

Topographic (i.e., form-drag) instability is one of the mechanisms proposed as playing an important role in atmospheric low frequency variability (e.g., Frederiksen 1983; Legras and Ghil 1985; Nathan 1988, 1989; Howell and Nathan 1990; Frederiksen and Bell 1987; Jin and Ghil 1990; Tribbia and Ghil 1990; O'Brien and Branscome 1991). Drs. Barcilon and Nathan conjecture that understanding block formation and demise may be linked to understanding low frequency dynamics. As originally shown by Charney and DeVore (1979), alteration of the zonal mean momentum will likely play an important role in topographically induced instabilities. This point is underscored by Nathan (1992), who analytically demonstrated within the context of the two-layer baroclinic model that steady, zonally varying potential vorticity (PV) sources can interact with the wave field to alter the zonal mean flow, resulting in dramatic changes in the linear topographic instability properties of the system. However, at finite-amplitude only steady solutions were obtained; the absence of perpetual, low frequency oscillations was attributed to the exclusion of wave-wave interactions within the model.

Under AFOSR Grant 49620-92-J-0498, Drs. Barcilon and Nathan are studying the impact of steady, zonally varying vorticity forcing on topographic instability and finite amplitude, low frequency oscillations. The model consists of a viscous, barotropic fluid on a zonally periodic, midlatitude $\beta$-plane channel, bounded above by a flat, rigid boundary, below by a bottom topography, and laterally by sidewalls at $y = 0,\ \pi$. For a steady, meridionally sheared basic flow $\overline{U}(y)$ the nondimensional equations governing the quasi-geostrophic dynamics of a superimposed disturbance, $\psi(x,y,t)$ and mean field, $\overline{\psi}(y,t)$, are:

$$\left(\frac{\partial}{\partial t} + \overline{U}\frac{\partial}{\partial x}\right)\nabla^2\psi + (\beta - \overline{U}_{yy})\frac{\partial\psi}{\partial x} + J(\psi,\ \nabla^2\Psi) + J(\psi,\ h_B) = -\gamma\nabla^2[\psi - \Psi(y)] - \overline{U}\frac{\partial h_B}{\partial x} + q_B\ , \tag{1a}$$

$$\frac{\partial}{\partial t}\frac{\partial^2\overline{\psi}}{\partial y^2} = -\gamma\frac{\partial^2\overline{\psi}}{\partial y^2} - \frac{\partial}{\partial y}\left(\overline{\frac{\partial\psi}{\partial x}h_B}\right) - \frac{\partial}{\partial y}\left(\overline{\frac{\partial\psi}{\partial x}\nabla^2\psi}\right) + \gamma\frac{\partial^2\Psi}{\partial y^2}\ , \tag{1b}$$

with $\psi_x = \overline{\psi}t = 0$ at $y = 0,\ \pi$. In these equations $h_B(x,y)$ is the bottom topography, $q_B(x,y)$ is a steady, ***zonally varying*** vorticity source, $\Psi(y)$ is an imposed perturbation zonal momentum drive and $\gamma$ measures the Ekman pumping strength on the upper and lower boundaries.

Equation (1*b*) indicates that changes in the mean flow vorticity are due to damping, topographic form drag, convergence of zonally rectified vorticity fluxes and externally imposed drive.

Nathan and Barcilon (1993) let $\overline{U}(y) = Ug(y)$, where $U$ is a characteristic zonal velocity, $h_B(x,y) = H(y)\{\tilde{h}e^{ikx} + *\}$ be the topographic forcing and $q_B(x,y) = Q(y)\{\tilde{q}e^{ikx} + *\}$ be the vorticity forcing. The forcing amplitudes $\tilde{h}$ and $\tilde{q}$ are assumed complex, thus allowing for a phase shift between the forcings. Then they let $\overline{U} = U_l(1+\eta)$, where $|\eta| \ll 1$ measures

the departure from linear resonance produced by the perturbation zonal momentum source $\Psi(y)$ and introduce the long time scale $\tau = \eta t$; the dissipation and forcing terms are ordered as follows $\gamma = \varepsilon^2 R$; $h_B = \varepsilon^3 h(x,y)$; $q_B(x,y) = \varepsilon^3 q(x,y)$; $(\psi) = \varepsilon^2 \Psi^{(2)}(y)$; $\varepsilon^2 = 0(\eta)$. They write

$$\psi(x,y,\tau) = \varepsilon\varphi_1(y)\{A(\tau)e^{ikx} + *\} + \varepsilon^2 F(y)\{A^2(\tau)e^{i2kx} + *\} + \varepsilon^2\varphi_0^{(2)}(y,\tau) \ . \qquad (2)$$

For arbitrary phasing between the topographic and vorticity forcings, the governing equations are non-separable in $y$ and $\tau$. To simplify the analysis, Nathan and Barcilon assume that the vorticity forcing is maximized either 90° upstream or 90° downstream of the topography; omitting the details reported in their paper, the governing equations are now of the form

$$\frac{dA}{d\tau} + RA + i\delta A + i\omega|A|^2 + iaZA - ib\tilde{h}_r + ib_2\tilde{q}_i = 0 \ , \qquad (3a)$$

and

$$\frac{dZ}{d\tau} + RZ = -A_i \ , \qquad (3b)$$

where all the coefficients are real and defined in their paper.

The second term in (3$a$) represents linear (Rayleigh) damping and the third term represents the linear frequency correction arising from the $O(\eta)$ departure of the basic flow from resonance. The first three terms alone yield a damped, slowly propagating Rossby wave. The fourth term is the nonlinear frequency correction arising from wave-wave interaction and is essential to the generation of low frequency oscillations. The fifth term represents wave-mean flow interaction. The last two terms are the forcings, which may augment or oppose each other depending on the spatial structures, strengths, and phasing. The strength of the topographic forcing, measured by $b$, is proportional to $U_1 k$ implying that the topographic forcing dominates over the vorticity forcing when the zonal winds are strong and the zonal wave scale short.

To illustrate the role of vorticity forcing on the topographically induced Hopf bifurcation, eqs. (3$a$) and (3$b$) are written as

$$\dot{X}_1 + RX_1 - (\delta + X_3)X_2 - \tilde{\omega}(X_1^2 + X_2^2)X_2 = 0 \ , \qquad (4a)$$

$$\dot{X} + RX_2 - (\delta + X_3)X_1 + \tilde{\omega}(X_1^2 + X_1^2) = 1 + \hat{q}_i \ , \qquad (4b)$$

$$\dot{X} + RX_3 = -cX_2 \qquad (4c)$$

where $X_1 + iX_2 = A/b\tilde{h}_r$, $X_3 = aZ$, $c = ab\tilde{h}_r^2$, $\tilde{\omega} = \omega(b\tilde{h}_r)^3$, and $\hat{q}_i = -b_2\tilde{q}_i/b\tilde{h}$. The dynamical system described by (4) was integrated numerically using a fourth order Runge-Kutta scheme; a nondimensional time step of 0.05 generally proved sufficient. For the cases presented below, Nathan and Barcilon have varied $\delta$ and $\hat{q}_i$ and set the remaining parameters and initial conditions equal to those used by Jin and Ghil (1990) in their Figs. 4–8: $c = 1.0$, $\omega = 0.5$, $R = 0.1$, $X_1(0) = X_2(0)$ and $X_3(0) = -4.8$.

Figure 1 summarizes the types of solutions that emerge from (4) for different combinations of $\delta$ and $\hat{q}_i$. The steady solutions are denoted by $S$. The oscillatory solutions are generally of two types. The first type, denoted by $P$, has been identified by Jin and Ghil (1990) and is characterized by a single, low frequency oscillation, which falls within the intraseasonal time scale. The second type, denoted by $T$, only arises for $\hat{q}_i > 0$, i.e., when the vorticity forcing augments the topographic forcing. The $T$-solutions are characterized by a very long oscillation within which is embedded two distinctly different regimes of behavior: a damped, low frequency amplitude oscillation in which the wave field propagates around the domain, and a state where the wave field remains quasi-steady. Only steady solutions exist for $|\delta|$ sufficiently large.

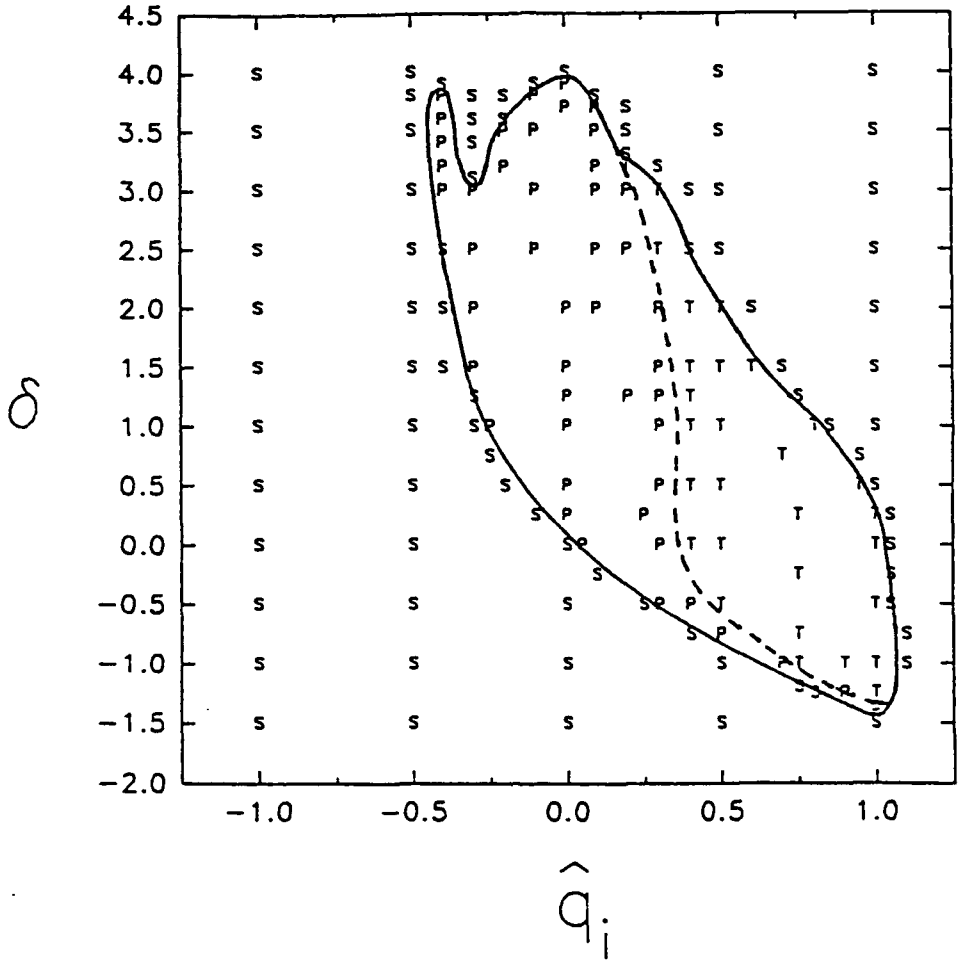


Figure 1: Mapping of the steady ($S$), low frequency oscillation ($P$), and two regime oscillation ($T$) solutions that arise for various combinations of $\delta$ and $\hat{q}_i$, where $\delta$ is proportional to the departure from topographic resonance and $\hat{q}_i$ is proportional to the amplitude of the vorticity forcing. The solid lines separates the steady and oscillatory solutions and the dashed line separates the single and two regime solutions. pw

Topographically induced low frequency oscillations in the presence of a steady, zonally

varying vorticity source have been studied. The source has been shown to interact with the perturbation field to produce zonally rectified wave fluxes that change the zonal momentum balance of the system. This change provides a mechanism for coupling the topographic and vorticity forcings, leading to a dramatic alteration in the Hopf bifurcation from stationary to low frequency, finite amplitude oscillations. In particular, Nathan and Barcilon have shown that the vorticity forcing is capable of generating low frequency oscillations that remain strictly upstream of the topographic ridge. For sufficiently large vorticity forcing, the Hopf bifurcation is destroyed, irrespective of the relative phase of the forcings. Nathan and Barcilon have obtained solutions that exhibit two distinctly different types of regimes. One regime is a westward-propagating, low frequency oscillation that has the character of a *free* wave. The second regime is characterized by a quasi-steady state in which the wave ridge remains upstream of the topographic ridge. Details are contained in the paper by Nathan and Barcilon (1993).

## 2. Use of Empirical Orthogonal Functions (EOFs) as Basis Functions

### a. Introduction

Lorenz (1956) first used empirical orthogonal functions (EOFs) as basis functions in the analysis of atmospheric data in place of tabulated functions, such as spherical harmonics. Typically, the number of EOFs required to represent 95% of the variance of a meteorological variable is about one third the number of degrees of freedom found in conventional numerical weather prediction models.

One of the disadvantages of EOFs is their lack of well defined functional forms and the associated difficulty in dealing with these functions in mathematical equations. Schubert (1985) showed that, with the use of spherical harmonics, it is possible, in part, to overcome this limitation by formulating the EOFs in the *spectral* domain and using spherical harmonic identities to simplify the mathematical expressions. Schubert developed a barotropic EOF forecast model that conserves either energy or enstrophy for the *truncated* EOF set; both energy and enstrophy are conserved if the *full* set of EOFs is used. Using 40 EOFs with an equivalent barotropic model, he found equally good correlations between the observed and EOF-modeled stream function tendencies as were found between observed and spectrally-modeled tendencies using 68 spectral coefficients.

Graduate student Y. Chang, in collaboration with Drs. Barcilon and Pfeffer, is applying the EOF methodology to a realistic, but idealized, *two-layer, baroclinic model* to understand the advantages and drawbacks of EOF modelling in numerical weather prediction. The EOF is based on very long model data sets generated using Dr. Whitaker's spectral model developed while he was a graduate student in our program (Whitaker 1990).

b. Summary of research in numerical prediction using EOFs

The words italicized below correspond to components in the block diagram displayed in Figure 2.

The two-layer baroclinic hemispherical primitive-equation *(spectral transform)* model has been used to generate 100 years of data. After subtracting the 100 year time mean from the data set, Mr. Chang computed a set of real EOFs for each field in each layer, which was used to construct the EOF model *(Basis Functions* and *EOF Model).* To examine the significance of the data set, he used the dominant variance rule (Rule N) and performed the *Random Test.* He also examined *Eigenvalue Resolution* which provides an approximation to the sampling error of the eigenvalues and eigenvectors of the covariance matrix. From the *Random Test* and *Eigenvalue Resolution* he obtained a measure of the number of EOFs needed.

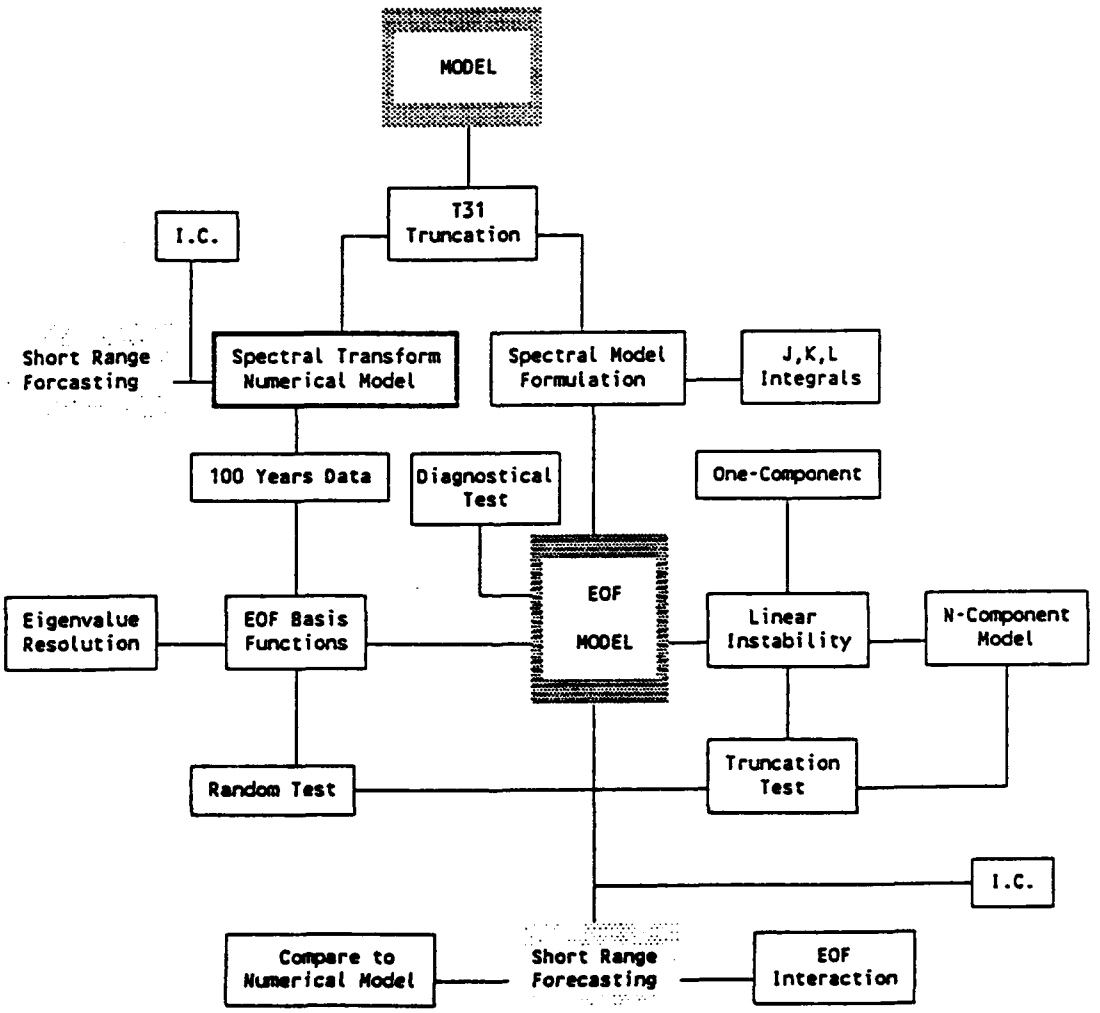


Figure 2.

The following presents in greater detail the work which is summarized in the preceding paragraph.

c. Data and data analysis

*c.1 Data:* Under the supervision of Drs. Barcilon and Pfeffer, Mr. Chang analyzed 100 years of data for stream function, velocity potential and the thickness for each layer. A spherical harmonic ($Y_n^m$) expansion was then performed with T31 truncation. The data consist of twice daily values of three variables for each layer in one hemisphere of the model. The bottom topography is a zonal wave number two mountain with peaks at 45 degrees latitude and the mountain height vanishing at the north pole and at the equator; its amplitude is 2 km. Figure 3 shows upper layer mean stream function and the variance of the meridional velocity $v$ for 100 years of data.

*c.2 Empirical Orthogonal Functions:* Chang, Barcilon and Pfeffer expand the data in spherical harmonics and write

$$F(\lambda,\ \mu,\ t) = \sum_{\gamma} F_\gamma(t) Y_\gamma(\lambda,\ \mu) \tag{3.2.1}$$

where $F_\gamma$ are the (complex) spectral transforms of amplitude (Platzman). We then seek an orthogonal function expansion of $F_\gamma(t)$ of the form (Schubert, 1985)

$$F_\gamma(t) = \sum_{k} z_k(t) E_k(\gamma)\ , \tag{3.2.2}$$

$E_k(\gamma)$ are the complex EOFs in the wave number domain which form a complete set, and are found by solving the appropriate eigenvalue/vector problem for the spectral coefficient covariances. The principal components (PCs), $z_k(t)$, are given by

$$z_k(t) = \sum_{\gamma} \overline{E_k}(\gamma) F_\gamma\ . \tag{3.2.3}$$

The upper layer streamfunction EOF structures are shown in Figure 4. EOF1 has a dominant zonal mean and wave number 2 pattern, and accounts for up to 11.4% of the total variance. It contains many of the features of the $\overline{v'^2}$ plots (Figure 3). EOF2 and EOF3 are associated with a traveling wave #5, and account for 15.4% of the variance. EOF4 and EOF5 produce a traveling wave #6 and represent 11.1% of the variance. The NS oriented dipole structures over the mountain-valley regions in EOF6 are believed to be related to blocking. EOF7 has important contributions from zonal wave number 2 in lower latitudes, zonal wave number 4 in midlatitudes and zonal wave number 0 in higher latitudes. EOF8 is made up predominantly of zonal wave number 1. This is reflected in the spatial pattern which is composed of 2 large anomaly centers of opposite sign on the two mountain ridges.

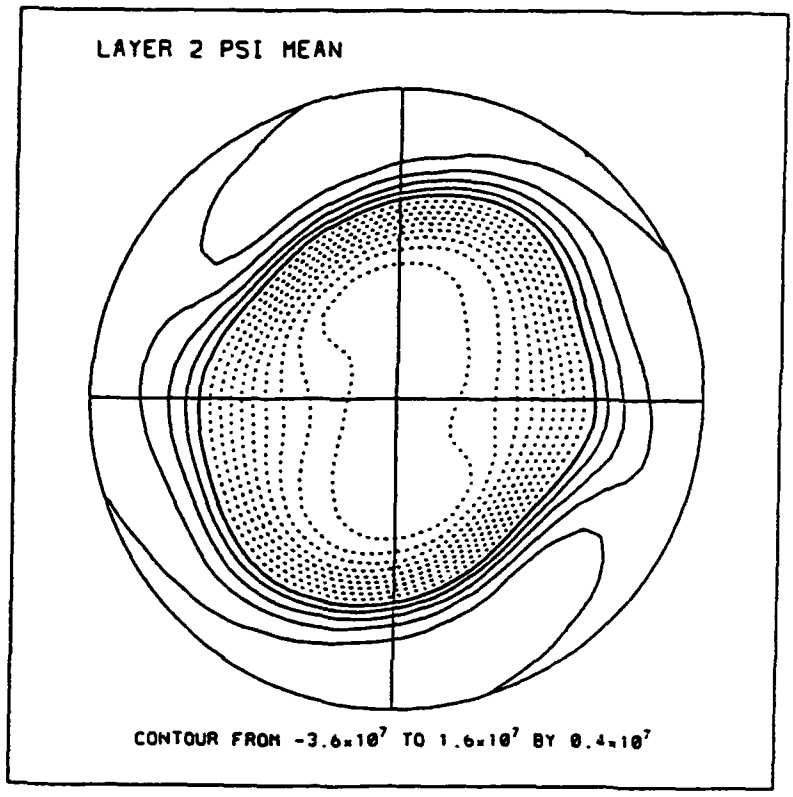


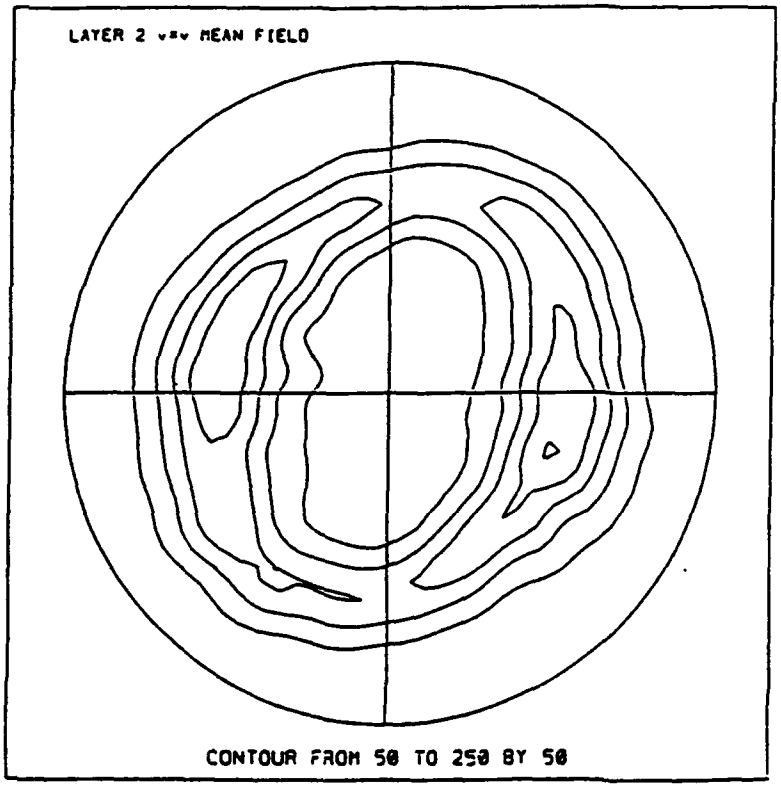


Fig. 3 a. Upper layer mean stream function. b. Variance $\overline{v'^2}$ of meridional velocity. In the figures, zero deg longitude is at 3 o'cl and the mountain peaks are at 45° and 135° longitude.

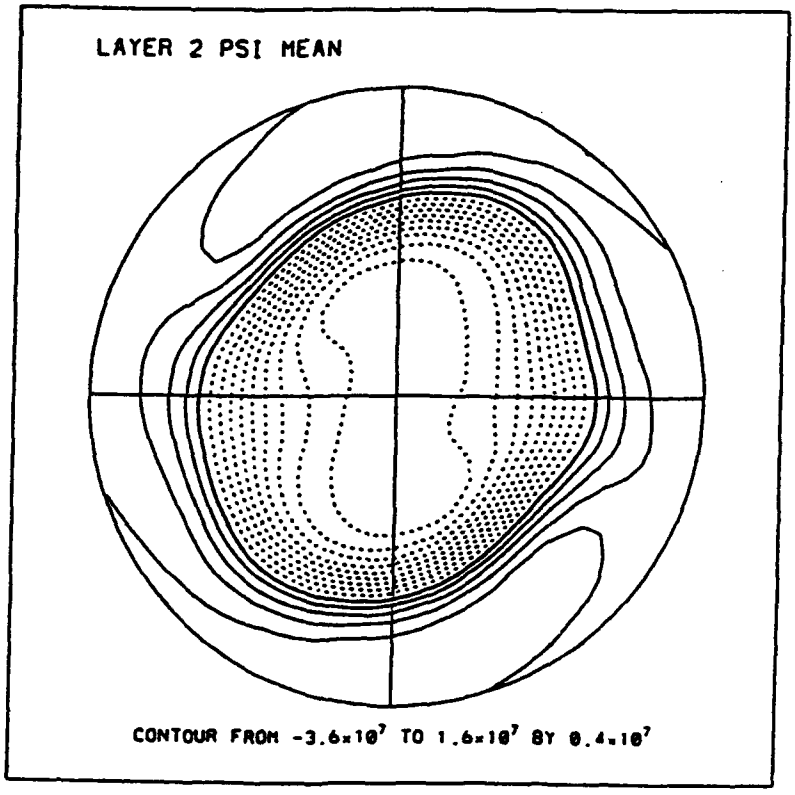


a.

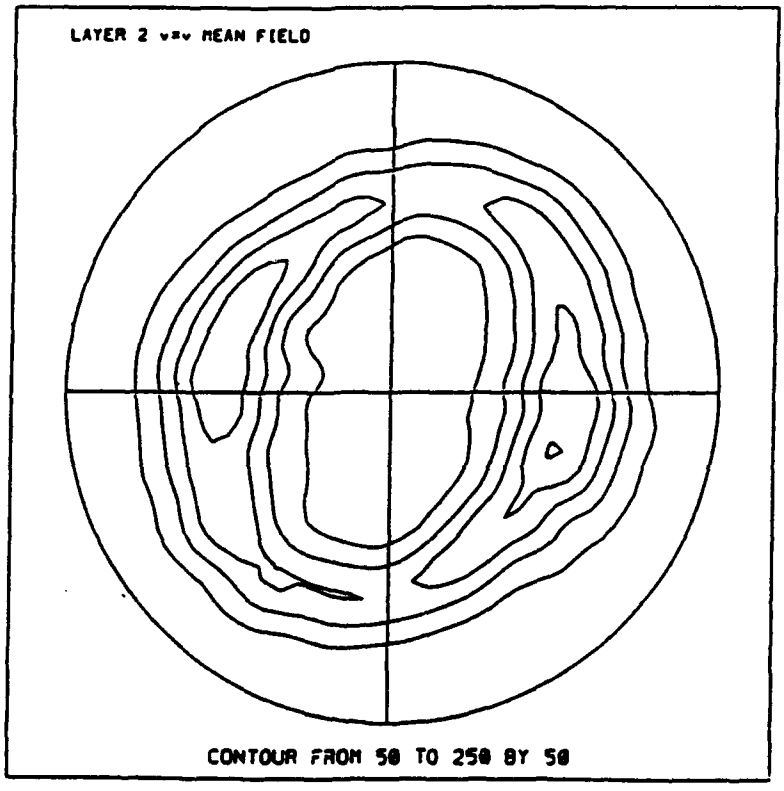


b.

Fig. 3 a. Upper layer mean stream function. b. Variance $\overline{v'^2}$ of meridional velocity. In the figures, zero deg longitude is at 3 o'clock and the mountain peaks are at 45° and 135° longitude.

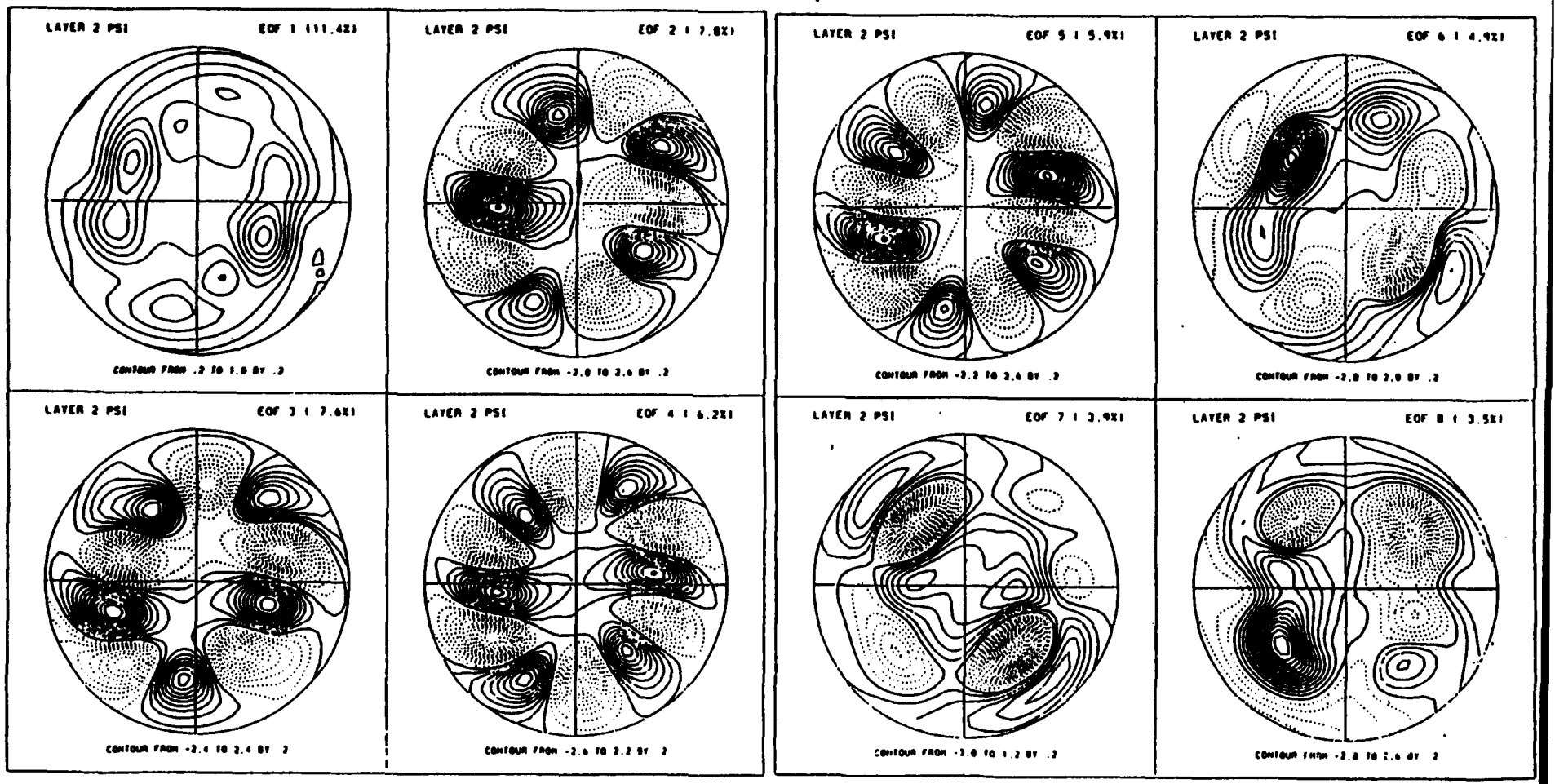


Fig. 4 EOFs of streamfunction $\Psi$ for the upper layer

*c.3 Selection Rule for Principal Component Analysis:* A given field $Z = z(x,t)$ can be represented as

$$z(x,t) = \sum_{j=1}^{P} \lambda_j^{\frac{1}{2}} \alpha_j(t) e_j(x) \ , \tag{3.3.1}$$

where $x = 1, ..., P$; $t = 1, ..., N$, and the sequence of eigenvalues is such that $\lambda_1 \geq ... \lambda_P \geq 0$. Generally, after a certain index $P'$, the magnitudes of the $\lambda_j$ drop abruptly and remain relatively small; therefore, only the first $P'$ eigenvalues may be considered important in the representation of the total variance of the data set (3.1.1). The remaining eigenvalues contain negligible variance and are difficult to differentiate from those generated by noise.

Chang, Barcilon and Pfeffer used data sets of length 100 years to test the significance of the truncated data set (Preisendorfer et al., 1981). They used the asymptotic behavior of random reference data test and compared the noise eigenvalues to the data eigenvalues. The 95% points on the cumulative distribution of the noise process (small dots) are shown in Figure 5. The data eigencurve (large dots) is shown cutting through the noise eigencurve. The data eigenvalues are no longer considered significantly greater than noise eigenvalues when found beneath that threshold. For the stream function field, the first 50 PCs have variability significantly larger than would be expected from a noise process. These modes, when added, explain about 90% of the variance.

d. The EOF model

*d.1 Model formulation:* Each quantity is expressed in terms of spherical harmonics and the orthonormality of $Y_\gamma$ is used to isolate the tendency equation for each component. The governing equations become

$$\begin{aligned} c_\gamma \dot{\psi}'_{n,\gamma}(t) &= F(\psi, \chi, Z) \ , \\ c_\gamma \dot{\chi}'_{n,\gamma}(t) &= G(\psi, \chi, Z) \ , \\ Z'_{n,\gamma}(t) &= H(\psi, \chi, Z) \ , \end{aligned}$$

where $\psi$ is the streamfunction, $\chi$ is the velocity potential and $Z$ is the layer thickness. The dot represents a time derivative. The spectral quantities are expanded in terms of EOFs as

$$\begin{aligned} \psi'_{n,\gamma}(t) &= \sum_k A_k^{(n)}(t) E_k^{\psi,n}(\gamma) \ , \\ \chi'_{n,\delta}(t) &= \sum_k A_k^{(n)}(t) E_k^{\chi,n}(\delta) \ , \\ Z'_{n,\delta}(t) &= \sum_k C_k^{(n)}(t) E_k^{\Delta Z,n}(\delta) \ , \end{aligned}$$

where $A_k^{(n)}(t)$ and $C_k^{(n)}(t)$ are the real PCs.

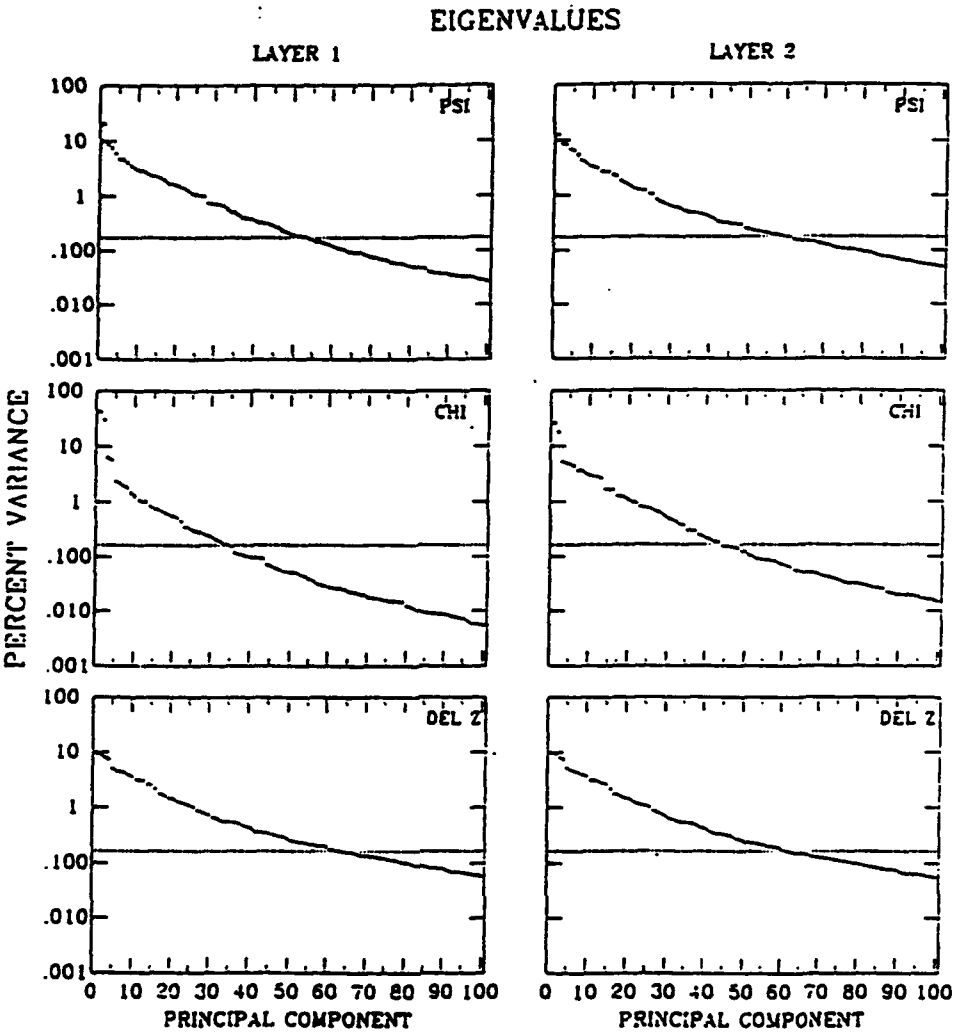


Fig. 5 Eigenvalues for EOFs 1 to 100, and 95% confidence limits.

After some manipulation, we obtain for, say the vorticity equation, an equation of the form:

$$\dot{A}_j^{(n)}(t) = \text{NL} + \text{Rotation} + \text{Mean/EOF} + \text{Dissipation},$$

where "Rotation" denotes a collection of terms involving the Coriolis and $\beta$ parameters, "Mean/EOF" denotes terms associated with the mean flow and EOF interactions and the other remaining symbols have standard meanings.

*d.2 Variance of the EOF model terms:* The standard deviations of the various terms in the model are calculated as a function of the PCs using a one year data set. The Spectral Transform Model (ST Model) tendency is computed from a centered finite difference formula. All other terms on the right hand side of that equation are computed by inserting the sampling values of the PCs into the EOF model terms.

Figure 6 shows the comparison between the standard deviation of the EOF Model

tendency and that of the ST Model for the vorticity equation for upper layer. There is a very good agreement for the PCs of the 50 EOF Model. In the upper layer, the dominant terms are the mean flow/EOF interactions and the Rotation term. These two terms are much larger than the tendency term in some large zonal wave number PCs, but are highly negatively correlated so that their sum has a much smaller standard deviation. Two large peaks occur in the mean flow/EOF term, one around the $2^{nd}$ , $3^{rd}$ , $4^{th}$ and $5^{th}$ PCs and others at the $10^{th}$ and $11^{th}$ PCs. The spatial distribution of the corresponding EOF patterns reveals very strong traveling waves with zonal wave number 5–7. The EOF interaction terms are smaller than the tendency for all components with the largest contribution coming from the $9^{th}$ component. The vertical advection term is at least one order of magnitude smaller than the tendency term for all the PCs.

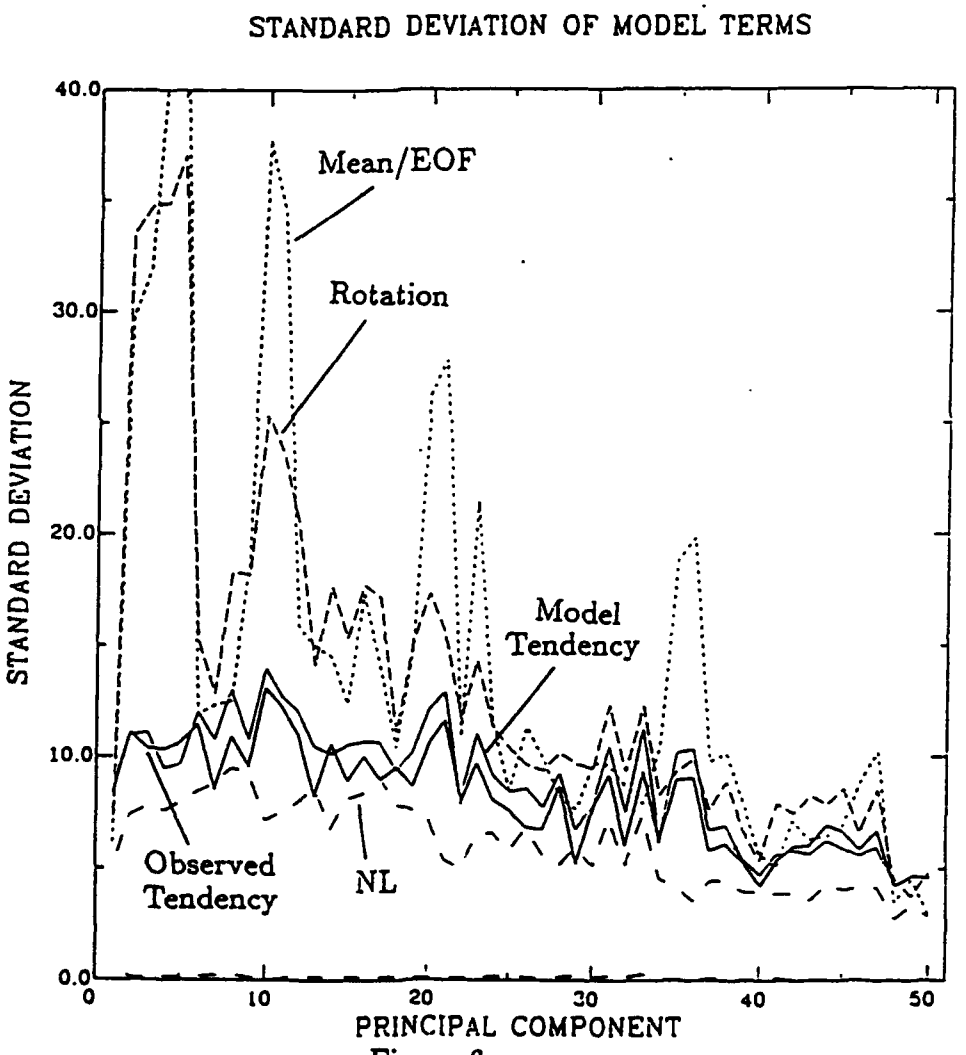

Figure 6.

*d.3 Tendency Correlations:* A simple measurement of the forecast skill of the EOF Model is to compute the correlations between the ST Model tendency and the EOF Model tendencies for each PC. The method we used here is identical to that of the previous

section.

Figure 7(a) shows the correlations as a function of PC for the models truncated at 50 PCs. The correlations are presented between ST Model tendency and Mean/EOF, EOF interactions and Rotation terms of the EOF Model. In the upper layer, one finds the Rotation term and Mean/EOF term are negatively correlated for most PCs. They have almost the same magnitude but opposite sign. The EOF interaction term is important in the upper layer. It has a correlation of 0.5 for the $2^{nd}$ and $3^{rd}$ PCs. This high correlation shows that the main contribution to the tendency comes from the nonlinear interaction terms.

Figure 7(b) shows the complete 50 PCs EOF Model tendency. In the upper layer, seven PCs have correlations greater than 0.8; these are the $2^{nd}$ , $3^{rd}$ , $5^{th}$ , $6^{th}$ , $8^{th}$ , $9^{th}$ and $10^{th}$ . There is a big drop in correlation amplitude when the EOF interaction terms are neglected. The results show a trend toward lower correlations with increasing PC number.

e. Future Work: See Figure 1 for a sketch of the future work which we propose to undertake next year.

## 3. Laboratory Model of Moist Convection and Parameterization in NWP

Dr. Ruby Krishnamurti is completing a paper entitled "Generation of low frequency modes in turbulent Rayleigh-Bernard convection", which will be submitted shortly to *J. Fluid Mech.*. This paper presents a mathematical model that accounts for a major new experimental result, namely the discovery that steady forced turbulent convection can spontaneously generate traveling organized structures, giving rise to a long period oscillation superimposed on the high frequencies usually associated with turbulent convection.

Dr. Krishnamurti has also designed and constructed an apparatus for measuring heat and momentum fluxes in an annulus of convecting fluid. In particular, the fluid is stably stratified by heating from above and cooling from below, but convects because of internal heat sources. The location of this internal heating is governed by the fluid flow itself: the working fluid is water containing a small amount of thymol blue which is normally used as a pH indicator. In its neutral state it makes the water appear orange, but with an excess of hydroxyl ions, it makes the water dark blue. In the present arrangement, the working fluid acts as a very weak electrolyte, its lower boundary acts as the positive electrode connected to a 9 volt battery. Near this lower boundary then, the water turns dark blue. Orange light from a sodium vapor lamp passes through the orange water with negligible absorption, but is strongly absorbed by the blue fluid which is thereby heated. (The instability of this heated layer is the subject of a paper entitled "Stability theory of an internally heated fluid layer" by R. Krishnamurti and S. Ranganathan.) Instability in this heated layer causes blue fluid to rise. However, as long as it remains blue, it continues to absorb radiation, continues to be heated and continues to rise. Thus the internal heat source is only in the rising, (not in the sinking) plumes.

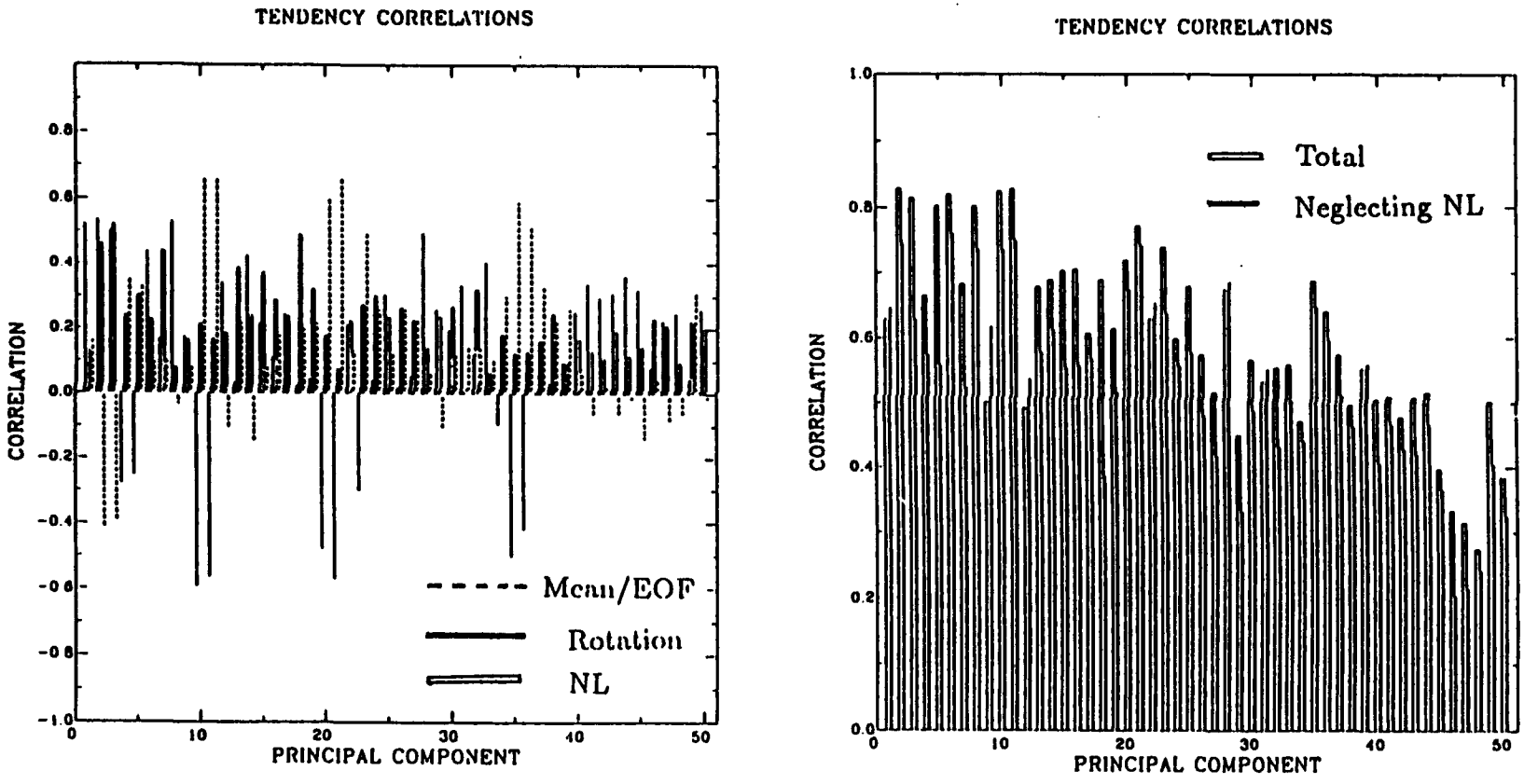


(a) (b)

Fig. 7 Correlation coefficients as a function of principal component.
a. Correlations between "observed" tendency and each term in the tendency equation.
b. Correlations between "observed" tendency and model tendency with and without nonlinear NL terms.

The bottom boundary is driven by a synchronous motor, providing a Couette flow with vertical shear. In this environment, the momentum transport, as well as the heat transport, by the convecting fluid will be measured. The apparatus should be operational by Fall 1993.

## D. Finite Element Model of the Shallow-Water Equations

A copy of the paper by Zhu, Navon and Zou submitted to *Mon. Wea. Rev.* is being sent under separate cover.

## References


Charney, J. G., and J. G. DeVore, 1979: Multiple flow equilibria in the atmosphere and blocking. *J. Atmos. Sci.*, **36**, 1205–1216.

Frederiksen, J. S., 1983: A unified three dimensional instability theory of the onset of blocking and cyclogenesis. *J. Atmos. Sci.*, **40**, 2953–2609.

Frederiksen, J. S., and R. C. Bell, 1987: Teleconnection patterns and the roles of baroclinic, barotropic and topographic instability. *J. Atmos. Sci.*, **44**, 2200–2218.

Howell, P., and T. R. Nathan, 1990: Barotropic instability of zonally varying flow forced by multimode topography. *Dyn. Atmos. and Oceans*, **15**, 35–58.

Jin, F.-F., and M. Ghil, 1990: Intraseasonal oscillations in the extratropics: Hopf bifurcation and topographic instabilities. *J. Atmos. Sci.*, **47**, 3007–3022.

Legras, B., and M. Ghil, 1985: Persistent anomalies, blocking and variations in atmospheric predictability. *J. Atmos. Sci.*, **42**, 433–471.

Lorenz, E. N., 1956: Empirical orthogonal functions and statistical weather prediction. *Sci. Rep.*, # 1, Dept. Meteor., MIT, 49 pp.

Nathan, T. R., 1988: Finite amplitude interaction between ustable baroclinic waves and resonant topographic waves. *J. Atmos. Sci.*, **45**, 1052–1071.

Nathan, T. R., 1989: On the role of dissipation in the finite amplitide interactions between forced and free baroclinic waves. *Geophys. Astrophys. Fluid Dyn.*, **45**, 113–130.

Nathan, T. R., 1992: The role of potential vorticity forcing in topographically induced instabilities. *Trends in Atmospheric Sciences*, (in press), Ed. E. Menon.

Nathan, T. R., and A. Barcilon, 1993: Low frequency oscillations of forced barotropic flow. To be published in *J. Atmos. Sci.*.

O'Brien, E., and L. E. Branscome, 1990: The effects of large-scale topography on the circulation in low-order models. *J. Atmos. Sci.*, **47**, 2597–2611.

Platzman, G. W., 1962: The analytic dynamics of the spectral vorticity equation. *J. Atmos. Sci.*, **19**, 313–328.

Platzman, G. W., F. W. Zwiers and T. P. Barnett, 1981: Foundations of princial component selection rules. *SIO reference series*, #18–4.

Schubert, S., 1985: A statistical-dynamical study of empirically determined modes of atmospheric variability. *J. Atmos. Sci.*, 42, (1), 3–17.

Tribbia, J. J., and M. Ghil, 1990: Forced zonal flow over topography and the 30-60 day oscillation in atmospheric angular momentum. NCAR Ms. 0501/98-5, 26 pp. [Available from National Center for Atmospheric Research, Boulder, CO.]